Pergamon

Geochimica et Cosmochimica Acta, Vol. 67, No. 16, pp. 2949–2963, 2003

0016-7037/03 $30.00 + .00

doi:10.1016/S0016-7037(03)00265-5

Experimental Study of Igneous and Sedimentary Apatite Dissolution: Control of pH, Distance from Equilibrium, and Temperature on Dissolution Rates

MICHAEL W. GUIDRY* and FRED T. MACKENZIE
Department of Oceanography, University of Hawaii, 1000 Pope Road MSB R204, Honolulu, HI 96822 USA

(*Received October* 30, 2002; revised 8 April 2003; *accepted in revised form April* 8, 2003)

Abstract—Apatite dissolution experiments were conducted using both a fluidized bed and stirred tank reactor over a range of pH, temperature, solution saturation state, and on non-carbonated and carbonated apatite compositions: igneous fluorapatite (FAP) and sedimentary carbonate fluorapatite (CFA), respectively. From 2 $<$pH $<$6, the rate of release from dissolution of all apatite components [calcium (Ca), phosphorus (P), and fluoride (F)] increased with decreasing pH for FAP. From 6 $<$ pH $<$ 8.5, the FAP dissolution rate is pH independent. Measuring apatite dissolution rates at pH $>$ 8.5 were not possible due to detection limits of the analytical techniques used in this study and the high insolubility of FAP. For the CFA compositions studied, the dissolution rate decreased with increasing pH from 4 $<$ pH $<$ 7. During early stages of the dissolution reaction for both FAP and CFA, mineral components were released in non-stoichiometric ratios with reacted solution ratios of dissolved Ca:P and Ca:F being greater than mineral stoichiometric ratios, suggesting that Ca was preferentially released compared to P and F from the mineral structure during the early stages of dissolution. An increase in reacted solution pH accompanies this early elevated release of Ca. As the dissolution reaction proceeded to steady state, dissolution became congruent. When normalized to BET measured surface area, FAP dissolved faster from 4 $<$ pH $<$ 7 compared to CFA. The apparent Arrhenius activation energy (E_a) of FAP dissolution over the temperature range of 25–55°C at pH = 3.0, I = 0.1, and pCO_2 = 0 is 8.3 ± 0.2 kcal mol^{-1}. Both the apparent exchange of solution H^+ for solid-bound Ca at low pH in the early stage of dissolution and the E_a of dissolution suggest a surface and not a diffusion controlled dissolution reaction for FAP and CFA. The degree of undersaturation of the solution, ΔG_R, with respect to FAP was important in determining the dissolution rate. At pH = 3.0, I = 0.1, and pCO_2 = 0, the dissolution rate of FAP was ~ 5× greater in the far-from-equilibrium region compared to the near-equilibrium slope region.

A simple apatite weathering model incorporating the experimental results from this study was constructed, and numerical calculations suggest that during the Phanerozoic both the surface area of igneous rock available for weathering and the average global temperature were important factors in determining the P weathering flux from apatite dissolution. It is possible that elevated global temperatures coupled with relatively high surface area of igneous rock during the early- to mid-Paleozoic resulted in elevated P weathering fluxes, which along with climatic evolutionary pressures of the Neoproterozoic, facilitated the radiation of multicellular organisms, large-scale phosphorite deposition, and abundance of calcium phosphate shelled organisms during the early Cambrian.

1. INTRODUCTION

Mineral dissolution and subsequent release of aqueous species play an important role in the cycling of elements. Mineral composition and environmental conditions can control the mechanism and rate of dissolution. The literature describing experimental studies of rates and mechanisms of the precipitation and dissolution of minerals is voluminous. Much experimental work on the kinetics of solution-mineral reactions has focused on silicate- (for a comprehensive review see White and Brantley, 1995; Pokrovsky and Schott, 2000; Oelkers and Schott, 2001; Oelkers, 2001) and Ca-Mg carbonate- minerals (e.g., Chou et al., 1989; Arvidson and Mackenzie, 1999; Pokrovsky and Schott, 2001). The kinetic properties of phosphate minerals including apatite have also been investigated, but not as extensively.

Until recently, the majority of research on apatite kinetics focused on compositional analogues for human dental or skeletal apatite (i.e., synthetic fluorapatite and synthetic hydroxyapatite) reacting under conditions that are appropriate to human biology (e.g., oral conditions of pH, salivary proteins, 37°C, etc.; Budz and Nancollas, 1988; Chin and Nancollas, 1991; Chin et al., 1993; Christoffersen et al., 1998) or non-stoichiometric solutions (Schaad et al., 1997). In one study of natural apatite dissolution, Dorozhkin (1997) investigated surface reactions of apatite briefly exposed to highly concentrated (2–7 mol/L) H_3PO_4 solutions. However, comparatively little effort has focused on how variations in temperature, solution composition (e.g., pH and saturation state), and mineral composition control the dissolution behavior of the geologically abundant igneous fluorapatite (FAP) and sedimentary carbonate fluorapatite (CFA) under the range of geologically relevant environmental conditions. One of the first kinetic studies of apatite germane to geologic applications was that of synthetic FAP precipitation from simple seawater solutions (Van Cappellen and Berner, 1991). However, for dissolution of geologically abundant apatite compositions of natural FAP and CFA under geologically appropriate conditions, there is little published kinetic dissolution research other than that of Lane and

* Author to whom correspondence should be addressed (mguidry@soest.hawaii.edu).

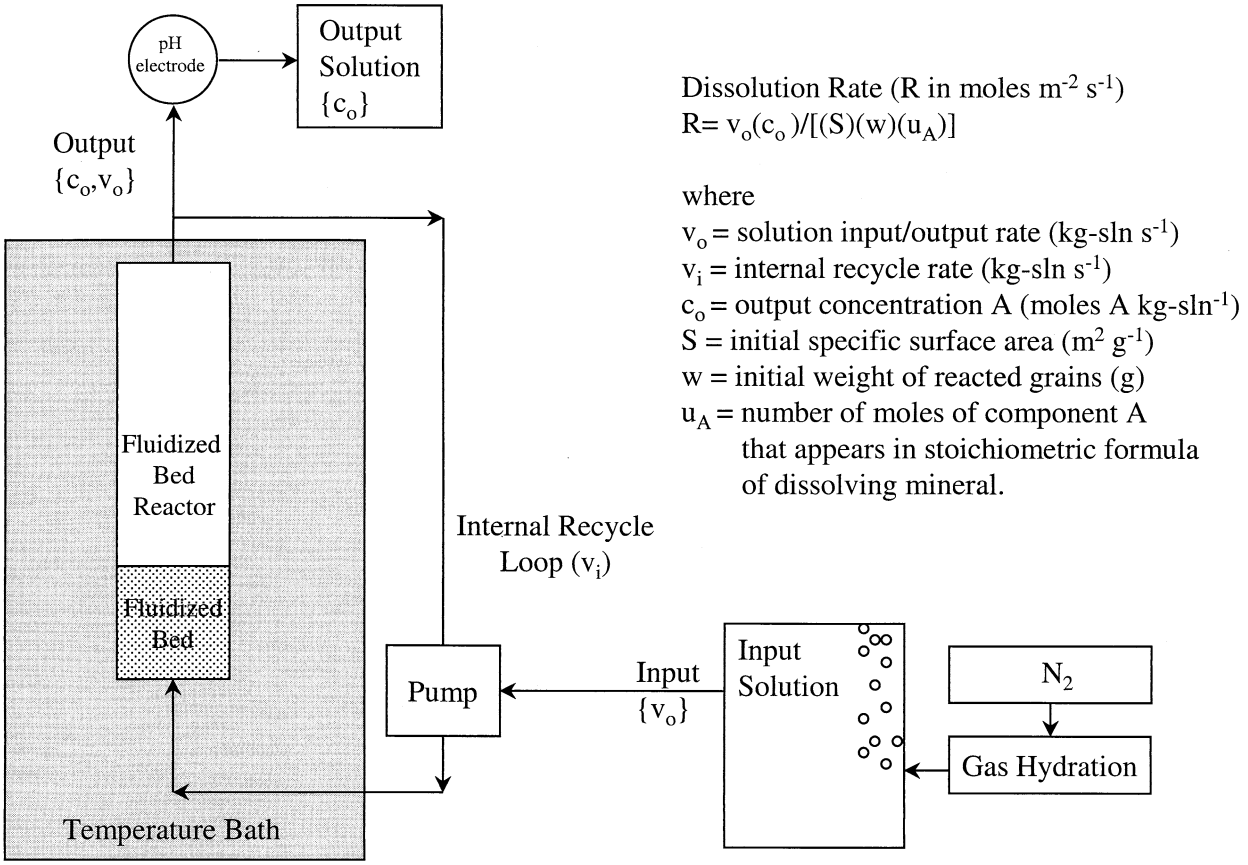

Fig. 1. Experimental fluidized bed reactor (FBR).

Mackenzie (1990, 1991), Tribble et al., (1995), Valsami-Jones et al. (1998), Guidry and Mackenzie (2000), and Welch et al. (2002).

A more in-depth investigation of the kinetic properties of FAP and CFA dissolution is presented here. Because apatite—in the form of FAP and CFA—is the primary exogenic phosphorus (P) sink (e.g., Froelich et al., 1982; Ruttenberg, 1993; Compton et al., 2000) and serves as the initial endogenic input of P to the earth's exosphere via the production of crystalline rock (e.g., Guidry et al., 2000; Guidry and Mackenzie, 2000), this work has relevance to the long-term P biogeochemical cycle in the exosphere. Dissolution of FAP and CFA also serves to replenish P lost from the exosphere via the subduction of ocean sediment and crust (Guidry et al., 2000). As such, the dissolution and weathering of apatite at the Earth's surface govern the release of P to both terrestrial and marine systems where it likely serves as a controlling nutrient on long-term net ecosystem production (e.g., Smith, 1984; Tyrrell, 1999).

2. MATERIAL AND METHODS

2.1. Experimental Design

Two experimental reactors—a fluidized bed reactor (FBR) and a stirred tank reactor (STR)—were used to carry out the dissolution experiments discussed in this paper. Figure 1 shows a diagram of the FBR. A single speed Techicon Proportioning Pump (Model II) peristaltic pump using different diameter tubing was used to control the input, output, and recycling rate of solution for the FBR. A chromatography column (Omnifit) with 5μm frits at both input and output to prevent the reacting apatite grains from escaping the reactor was used to suspend the grains in a fluidized bed. For general discussions of FBRs and their use in mineral kinetic studies see Chou and Wollast (1984), Chou (1985), Arvidson (1998) and Arvidson and Mackenzie (1999). The total volume of the FBR setup is $\sim$ 60ml. The input and output rate of fluid for both FBR and STR was controlled with the above-mentioned peristaltic pump. A peristaltic pump also controlled the internal recycling rate of the FBR system, which varied from 17.4 to 26.1 mL/min to create a fluidized bed and to ensure a well-mixed internal volume. The STR is depicted in Figure 2. A suspended stir bar was used to prevent grinding of grains within the reactor and to ensure proper mixing of the solution. The total volume of the STR is $\sim$ 60 mL. A frit placed at the STR output prevented mineral grains from leaving the reactor. A temperature bath regulated the reaction temperature of both FBR and STR to $\pm$ 0.1°C. The FBR was used to explore the effect of pH on the dissolution rate of FAP and CFA at acidic to neutral pH values (2–7). The STR was used to determine the effects of apparent activation energy, degree of undersaturation, and slightly acidic to basic pH conditions (6–8.5) on the dissolution rate of FAP.

For the degree of undersaturation and apparent activation energy experiments, the STR was more suitable than the FBR. This was due to the ability of the STR to mix instantaneously reacted solution with newly introduced non-reacted solution. The FBR experimental design required relatively long residence times and rapid internal recycling rates to ensure proper mixing so that the output solution was representative of the solution within the reactor. When input pump rates are relatively high compared to the recycling pump rates, concentration differences can result between the fluid exiting the FBR proper, the

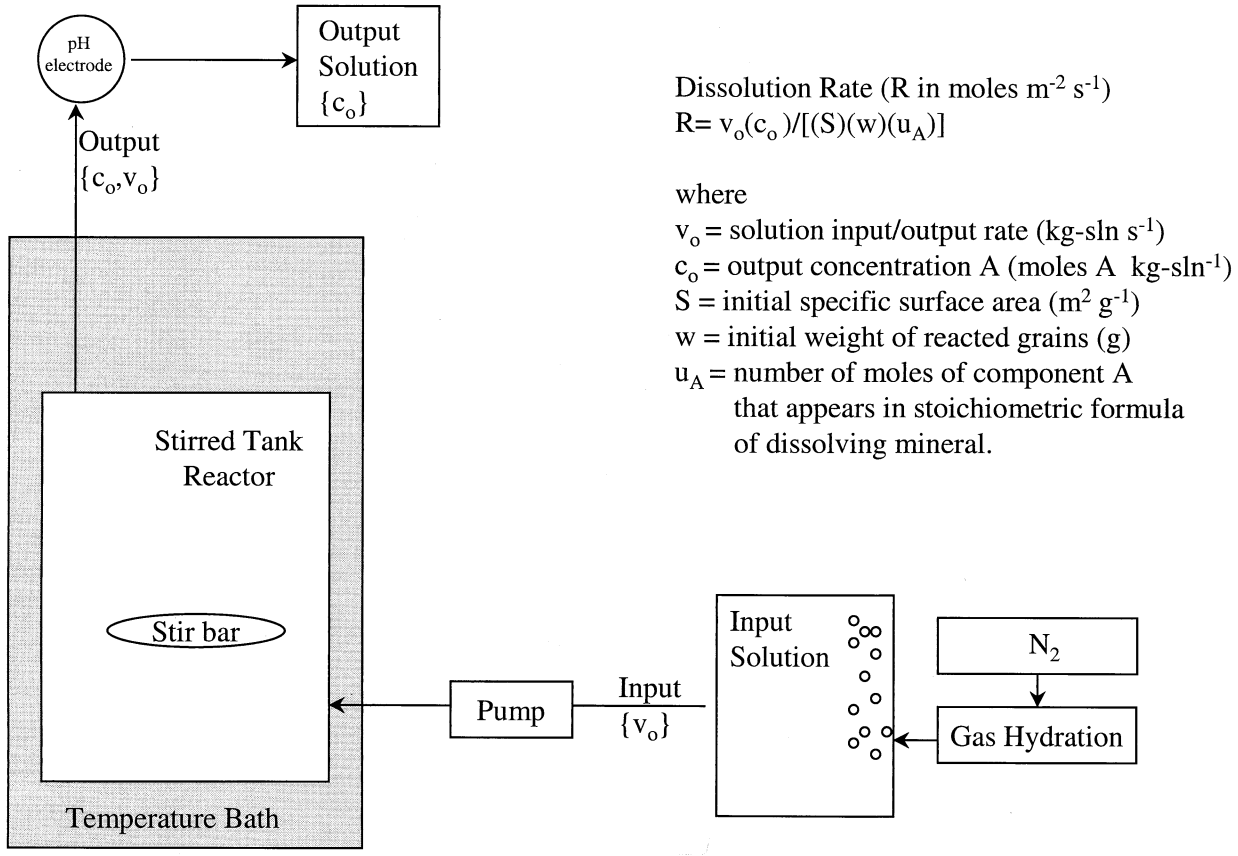

Fig. 2. Experimental stirred tank reactor (STR).

fluid in the remainder of the recycling loop, and wherever the fluid is sampled. The STR overcomes this problem because the stir bar nearly instantaneously mixes incoming non-reacted solution with the reacted solution. This is especially important when high fluid input rates are needed to minimize reaction times to achieve elevated degrees of undersaturation.

The STR was also used for studying the dissolution rate at $6 < pH < 8.5$ for FAP. Dissolution rates over this pH range were relatively slow. Unless sufficient solid was used in the reaction, the analytical methods employed were not able to discern differences between input and output solution composition. The FBR was not capable of containing enough solid over these conditions to measure a dissolution rate whereas the STR was able to accommodate enough solid. The FBR was used in lower pH, relatively fast dissolution experiments when possible because it ensures minimal abrasion of grains. Grain abrasion can be a problem in STRs that do not use suspended stir bars to mix the solution and reacting grains. At $pH > 8.5$, solution concentrations of Ca, P, and F that are resolvable by the analytical techniques used in this study resulted in a solution that was either saturated or slightly undersaturated with respect to apatite. Thus, it was not possible to measure dissolution rates at $pH > 8.5$ in either reactor. Using Eqn. 3, the calculated distance from equilibrium or Gibbs free energy of reaction, ΔG_R, of solution with Ca, P, and F = 5, 3, and 1 μmoles kg sln^{-1} at pH = 9.0 is only -1.24 kcal mol^{-1} or very close to equilibrium.

In general, FAP is less substituted in composition compared to CFA and is an end-member of apatite compositions (Jarvis et al., 1994). With this in mind, the purpose of the FAP experiments in this study is two-fold. First, it is to elucidate how pH, temperature, and degree of undersaturation impact FAP dissolution. Second, the FAP results serve as a reference for comparison with the CFA dissolution experiments of this study and subsequent more detailed future ones on CFA kinetic properties.

2.2. Apatite Seed Preparation

High purity research grade Durango igneous FAP was purchased from Ward's Scientific®, and the CFA samples used in the experiments were obtained from the Museum of Natural History, Washington, D.C. The FAP was crushed by hand under methanol using an agate mortar and pestle. CFA samples were not crushed to prevent alteration of surface properties before running the experiments. CFA samples were cleaned with sodium hyperchloride solution (Chlorox ©) to remove any residual organic material. All apatite grains were sieved to collect a specific size fraction of 106–212 μm and then ultrasonically cleaned in a methanol bath. This process was repeated until a clear supernatant was obtained. The apatite samples were then dried at room temperature. Subsequent analysis of the apatite grains by SEM showed that the sonication process had removed any preexisting fines and those created from the crushing process.

2.3. Apatite Seed Characteristics

Five apatite compositions were used in the dissolution experiments (Tables 1 and 2). Four of the compositions are sedimentary in origin and the other is igneous. The four sedimentary apatites were chosen using sample purity and carbonate weight percent as selection criteria. Sample purity was determined by X-ray diffraction and microwave acid digestion and solution analysis of the apatite sample. CuK_α radiation was used to scan samples within the range of 2° to 60° 2θ; this 2θ range includes the diffraction peaks for structural carbonate in apatite ({002}, {300}, {410}, and {004}) and the most common accessory minerals. The equations of Gulbrandsen (1970) were used to determine the degree of CO_3 substitution in the CFA samples. It is important to determine sample purity because all natural CFA samples consist of multiple phases. The sedimentary samples chosen for dissolution con-

Table 1. Sample ID, origin, form, genetic classification, grain size, and surface area of apatite compositions used in dissolution experiments.

Sample	Sample ID	Origin	Form	Genetic Classification	Grain Size (μm)	SA* ($m^2\ g^{-1}$)
CFA	CFA-3	Bau Craa, Spanish Western Sahara	Pellets	Sedimentary	212–106	6.8 ± 0.14
CFA	CFA-9	Tenonoc Mine, Florida	Pellets	Sedimentary	212–106	16.0 ± 0.20
CFA	CFA-10	Homeland, Florida	Pellets	Sedimentary	212–106	8.1 ± 0.16
CFA	CFA-1	Metlaoui, Tunisia	Pellets	Sedimentary	212–106	9.1 ± 0.30
FAP	FAP	Durango, Mexico	Crystals	Igneous	212–106	0.026 ± 0.0006

* Non-reacted surface area.

tained the phases CFA and minor quartz (SiO_2) in detectable amounts. The existence of quartz does not interfere with experimental results because the quartz content is minor (2–3 wt. %); quartz is relatively inert at acidic to pH < 9.6; and dissolved silica species do not interfere with the chemical analytical techniques used in this study. The surface areas of the non-reacted apatite compositions were determined by multipoint BET using Krypton gas (Table 1).

2.4. Input Solutions and Analytical Methods

Input solutions of two different ionic strengths (0.1 and $\leq$ 0.002) using reagent grade NaCl were prepared and the desired input solution pH was fixed by adding the appropriate amount of reagent grade HCl or NaOH. The FAP experiments were performed at I = 0.1, which allowed direct comparison with the few previously published natural FAP studies conducted at the same ionic strength (Wu et al., 1991; Valsami-Jones et al., 1998). In addition, the relatively high ionic strength helped 1) to reduce the effect of dissolution on changing ionic strength, complicating experimental results at relatively low pH, and 2) to provide stable pH measurements in the neutral to basic pH range. The preliminary CFA experiments were performed at low ionic strength ($\leq$0.002), approximating the low ionic strength characteristics of ground and river water. The non-reacted input solution was bubbled with presaturated N_2 to purge the input solution of CO_2.

Output reacted solution samples were collected in acid washed polyethylene bottles and were analyzed for aqueous calcium, phosphate, and fluoride concentrations. Calcium was measured by potentiometric titration using EGTA with a detection limit and uncertainty of 1 μmole Ca kg-sln^{-1} and 3%, respectively (Arvidson, 1998); phosphorus was measured colorimetrically using the molybdate blue method with a detection limit of 0.1 μmole P kg-sln^{-1} and uncertainty of 2% (Koroleff, 1983); fluoride was measured with a fluoride specific ion electrode using TISAB II to buffer pH with a detection limit of 1 μmole F kg-sln^{-1} with an uncertainty of 2% (Warner 1969; 1973; Froelich et al., 1983). All standards for aqueous species measurement were prepared with analytical grade reagents. The pH of the input and output solution was measured by using a pH electrode in a closed cell calibrated with NBS buffers to an uncertainty of $\pm$0.01.

2.5. Degree of Undersaturation Calculation

To determine thermodynamically whether there is the possibility for precipitation or dissolution of a mineral in solution, one must first calculate the saturation state Ω of the solution with respect to the mineral:

$$\Omega = \frac{IAP}{K}, \tag{1}$$

where IAP is the ion activity product calculated from solution composition, and K is the thermodynamic equilibrium constant of the mineral. The IAP was computed for FAP and CFA respectively using the following equilibrium reactions:

$$Ca_{10}(PO_4)_6F_2 + 6H^+ \overset{K}{\rightleftharpoons} 10Ca^{2+} + 6HPO_4^{3-} + 2F^- \tag{2}$$

and

Table 2. Carbon content, calculated stoichiometry, and measured stoichiometric ion ratios of apatite compositions used in the dissolution experiments [using formula of McClellan and Lehr (1969)].

Sample ID	Wt. % CO_2[1,2]	Calculated stoichiometry[3] (carbonated apatites only)	Ca:P[4,5]	P:F[4,5]	Ca:F[4,5]
FAP	0	$Ca_{10}(PO_4)_6F_2$	1.67[4]	3.0[4]	5.0[4]
			1.72[5] (±0.05)	3.03[5] (±0.09)	5.19[5] (±0.15)
CFA-3	2.15[1]	$Ca_{9.66}Mg_bNa_c(CO_3)_{0.48}(PO_4)_{5.52}F_{2.19}$	1.75[4]	2.52[4]	4.41[4]
	2.36[2]		1.76[5] (±0.05)	2.61[5] (±0.07)	4.61[5] (±0.13)
CFA-9	3.77[1]	$Ca_{9.55}Mg_bNa_c(CO_3)_{0.84}(PO_4)_{5.16}F_{2.34}$	1.85[4]	2.21[4]	4.09[4]
	4.18[2]		1.88[5] (±0.05)	2.23[5] (±0.06)	4.19[5] (±0.12)
CFA-10	4.37[1]	$Ca_{9.54}Mg_bNa_c(CO_3)_{0.97}(PO_4)_{5.03}F_{2.39}$	1.89[4]	2.11[4]	3.98[4]
	4.85[2]		1.99[5] (±0.06)	2.03[5] (±0.06)	4.03[5] (±0.11)
CFA-1	5.79[1]	$Ca_{9.42}Mg_bNa_c(CO_3)_{1.27}(PO_4)_{4.73}F_{2.51}$	1.99[4]	1.89[4]	3.76[4]
	6.45[2]		2.04[5] (±0.06)	1.89[5] (±0.05)	3.86[5] (±0.11)

[1] Determined from equation given in Gulbrandsen (1970).

[2] Determined from equation given in Schuffert et al., (1990).

[3] Determined from $Ca_aNa_xMg_y(CO_3)_z(PO_4)_{6-z}F_{0.4*z}F_2$ (after McClellan, 1980) where a = (2*z + 3*(6 − z) + (2 + 0.4*z) − × − 2*y)/2, b and c equal the number of moles of Mg and Na respectively, and where x and y are the average values of Mg (0.2) and Na (0.1) respectively of 16 sedimentary apatites (McClellan and Lehr, 1969). z was determined so that the composition's calculated wt. % CO_2 equals that of the composition's analytically determined wt. % CO_2 by XRD using the equation of Gulbrandsen (1970). FAP stoichiometry is from theoretical assumptions.

[4] Stoichiometric ratios derived from theoretical FAP stoichiometry.[3]

[5] Stoichiometric ratios derived from analytical measurement of ions in solution from the dissolution of bulk solid in acid with associated uncertainty—one standard deviation—in the stoichiometric ratio.

$$Ca_{10}(PO_4)_{5.83-0.57x}(CO_3)_xF_{2.52-0.3x} + H_2O \overset{K}{\rightleftharpoons} 10Ca^{2+} + (5.83 - 0.57x)\,PO_4^{3-} + (x)CO_3^{2-} + (2.52 - 0.3x)\,F^-. \quad (3)$$

For all experiments, ΔG_R of the reacted solution with respect to FAP and CFA and other possible secondary precipitate minerals was calculated using the solution modeling software EQ3 (Wolery, 1992). The solubility determination of laboratory synthesized CFA (log K = −107.5 to −122.0) by Jahnke (1981, 1985), which varies depending on the amount of carbonate ion substitution, was used to calculate the saturation state of reacted solution with respect to CFA. The equilibrium constant (log K = −49.98) for FAP from Robbie et al. (1979) was used to calculate the saturation state of reacted solution with respect to FAP. Using Ω, the Gibbs free energy of the total reaction, ΔG_R (kcal mol^{-1}) was computed:

$$\Delta G_R = 2.303 R_g T \log \Omega, \quad (4)$$

where

R_g = gas constant (1.987 cal mol^{-1} K^{-1})
T = temperature (K)

From undersaturated conditions, as the concentration and thus activity of an element in solution increases, the difference in chemical potential between the solid and the solution decreases and the solution approaches equilibrium. If the mass transfer, or flow, rate is sufficient to remove released elements from the solution immediately near the solid phase, the difference in chemical potential between phases will be maintained and element release will continue. Until recently, most mineral dissolution rates studies have been conducted in dilute solutions where they are relatively fast and easy to measure.

2.6. Dissolution Rate Calculation

To determine from experimental data the apatite dissolution rate, R(moles m^{-2} s^{-1}), the following equation was used:

$$R = \frac{v_0(c_0 - c_i)}{[(S)(u_A)]}, \quad (5)$$

where

v_o = solution input rate (kg-sln s^{-1})
c_i = input concentration of component A (mol kg-sln^{-1})
c_o = output concentration of component A (mol kg-sln^{-1})
S = BET determined initial specific surface area (m^2)
u_A = moles A per mol mineral dissolved.

Because the input concentration, c_i, for all experiments was zero, (5) can be reduced to:

$$R = \frac{v_o(c_o)}{[(S)(u_A)]}. \quad (6)$$

3. RESULTS AND DISCUSSION

3.1. Congruency of the Dissolution Reaction

Figures 3a and 3b depict typical results from FAP and CFA dissolution experiments at low to moderate pH (2 < pH < 5). Initially in the dissolution of FAP, there was a rapid release of components Ca, P, and F to solution reaching maximum concentrations during the first hours of the experiment. After the initial release and peak in concentration, there was then a decline in concentrations until the release rate of mineral components becomes constant after about 1–3 days. Initially for CFA, there was an increase in Ca, P, and F concentrations until steady state was reached after 1–2 days. Comparing the dissolved component concentrations versus time trend of CFA to FAP, there was no peak in concentration during the very early

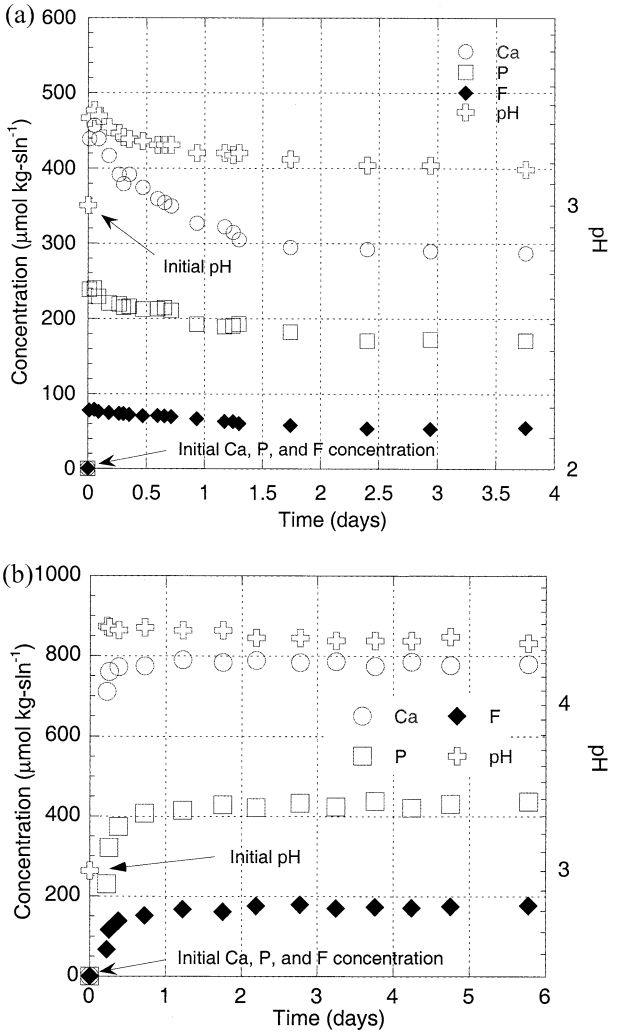

Fig. 3A. Calcium, phosphorus, fluoride, and pH vs. time for experiment FAP-B. The initial reactor solution concentration of calcium, phosphorus, and fluoride is 0 at t=0, which is the point that unreacted input solution is introduced to the solid within he reactor. Steady state for the dissolution reaction (over the duration of the experiment) is reached by the second day. Figure 3B. Calcium, phosphorus, fluoride, and pH vs. time for experiment CFA-3A. The initial reactor solution concentration of calcium, phosphorus, and fluoride is 0 at t=0, which is the point that unreacted input solution is introduced to the solid within the reactor. Steady state for the dissolution reaction (over the duration of the experiment) is reached by the second day.

stage of the experiment with CFA followed by a decrease to steady state.

The ratios of dissolved FAP and CFA constituents in solution for the experiments in Figures 3a and 3b are shown in Figures 4a and 4b. During the initial experimental stage, there are greater Ca:P and Ca:F ratios compared to stoichiometric mineral ratios for both FAP and CFA, an indication that Ca was being released in stoichiometric excess relative to P and F. During the first day of the experiments, there was a concomitant increase in pH and solution Ca concentration. A similar phenomenon was observed in silicate dissolution experiments (e.g., albite) at acidic pHs where mineral-bound cations are exchanged with hydrogen ions in solution and released to

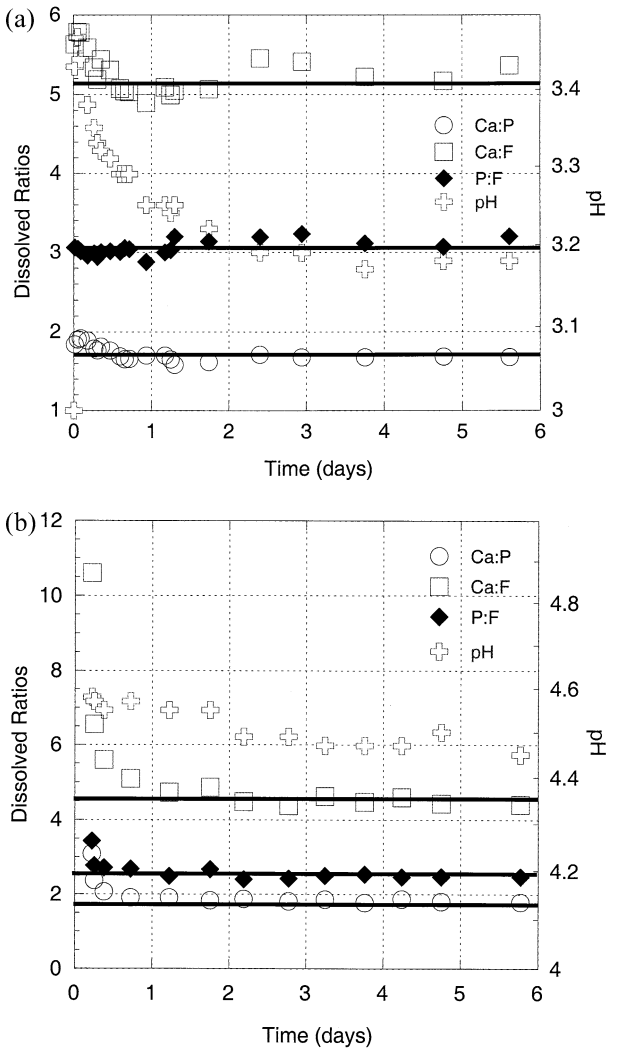

Fig. 4A. Ratios of dissolved constituents vs time for dissolution experiment FAP-B. The three solid horizontal lines represent the chemically measure stoichiometric ratios of Ca: P (1.72), Ca: F (5.19), and P: F (3.03) of the bulk mineral solid (Table 2). Compared to measured mineral stoichiometry, there is elevated release to solution of Ca relative to P and F during the early stages of dissolution. Input solution pH was 3.0 at t = 0 and sharply increased to almost 3.50 during the early stages of dissolution. The concurrent sharp increase in pH and elevated Ca: P and Ca: F ratios suggest that mineral bound Ca is being exchanged for solution hydrogen ion during the early stages of the dissolution reaction. Figure 4B. Ratios of dissolved constituents vs time for dissolution experiment CFA-3A. The three solid horizontal lines represent the chemically measure stoichiometric ratios of Ca: P (1.76), Ca: F (4.61), and P: F (2.61) of the bulk mineral solid (Table 2). Compared to measured mineral stoichiometry, there is elevated release to solution of Ca relative to P and F during the early stages of dissolution. Input solution pH was 3.0 at t = 0 and sharply increased to almost 3.50 during the early stages of dissolution. The concurrent sharp increase in pH and elevated Ca: P and Ca: F ratios suggest that mineral bound Ca is being exchanged for solution hydrogen ion during the early stages of the dissolution reaction.

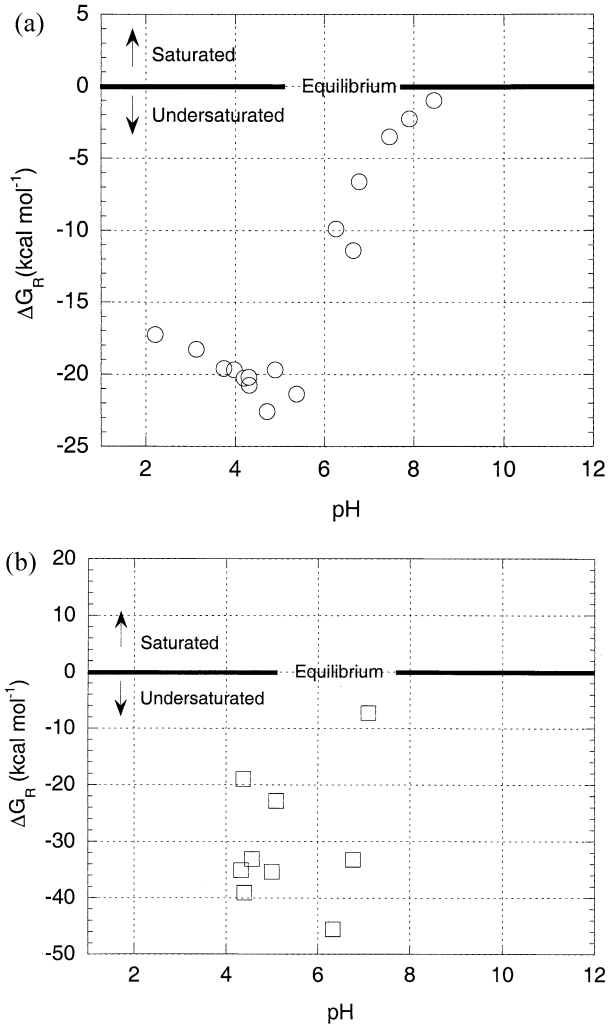

Fig. 5A. ΔG_R for FAP dissolution rate vs. pH experiments. Figure 5B. ΔG_R for CFA dissolution rate vs. pH experiments.

solution resulting in the concomitant increase of solution cation concentrations and pH (Chou and Wollast, 1984; 1985). Subsequently, a hydrogen-rich, cation-deficient surface phase was formed (Chou and Wollast, 1984; 1985). In this study, after a similar initial reaction phase, pH, Ca, P, and F concentrations decreased until reaching, for the duration of the experimental run, steady-state values that show the bulk mineral dissolution reaction was stoichiometric. The trends in solution Ca:P, Ca:F, and pH are similar to those of our previous work (Tribble et al., 1995) on CFA dissolution. We found that during the early stages of dissolution at acidic pH, Ca was released in excess of P and F compared to mineral stoichiometric ratios. After this early stage of dissolution, the solution ratios tended to congruent values indicating that the bulk mineral dissolution reaction was stoichiometric. For all dissolution rate versus pH experiments, the degree of saturation of the reacted solution with respect to FAP and CFA was calculated and all of the experimental solutions were found to be undersaturated (Figs. 5a and 5b).

3.2. Dissolution Rates

A series of experiments was run at 25°C from $2 < pH < 8.5$, $pCO_2 = 0$, and $I = 0.1$ to investigate FAP dissolution rates as

Table 3. FAP and CFA experimental dissolution data at 25°C and 1 atm. Solid is the amount in grams of FAP or CFA used in the dissolution experiment. Input rate is the rate at which non-reacted fluid is pumped into the stirred tank reactor or the internal recycle loop of the fluidized bed reactor. Input pH and output pH are the pH of the non-reacted and reacted solution respectively. Ionic strength is the ionic strength of the solution. Grain size is the mesh size of the seed used for the experiment. Grain size of FAP and CFA for all experiments is 106–212 μm. Mineral dissolution rates (mol m^{-2} s^{-1}) and distance from equilibrium (kcal mol^{-1}) are calculated at steady state using calcium, phosphorus, and fluoride measurements. At steady state, the dissolution reaction is stoichiometric.

Exp.	Solid (g)	Input rate (g min^{-1})	pH		Ionic Strength	Steady State Ca, P, and F (μmol kg-sln^{-1})			Log Rate (mol m^{-1} s^{-1})	ΔG_R (kcal mol^{-1})
			Input	Output		Ca	P	F		
FAP-A*	1.00	0.39	2.02	2.20	0.1	2423	1421	471	−6.91	−17.3
FAP-B*	1.00	0.37	3.00	3.15	0.1	240	148	50.1	−7.89	−18.3
FAP-C*	1.00	0.32	3.88	3.95	0.1	70.1	41.4	13.5	−8.57	−19.7
FAP-D*	1.00	0.80	4.00	4.20	0.1	42.7	25.9	8.5	−8.77	−20.3
FAP-E*	1.00	0.32	4.10	4.31	0.1	36.1	21.2	6.9	−8.79	−20.2
FAP-F*	1.00	0.27	4.56	4.90	0.1	18.6	11.1	3.7	−9.30	−19.7
FAP-G*	1.00	0.33	5.22	5.38	0.1	8.1	4.9	1.6	−9.42	−21.4
FAP-H	1.00	0.52	3.51	3.75	0.1	95	55	18.8	−8.15	−19.6
FAP-I	1.00	0.54	4.16	4.37	0.1	28	16	5.7	−8.67	−20.8
FAP-J	1.00	0.53	4.50	4.72	0.1	11.9	6.9	2.3	−9.02	−22.6
FAP-K	4.00	0.23	7.86	7.90	0.1	9	5.3	1.8	−10.1	−2.3
FAP-L	4.90	0.23	6.50	6.65	0.1	6.2	3.5	1.2	−10.4	−11.4
FAP-M	7.50	0.25	8.45	8.52	0.1	8.6	5	1.7	−10.4	−0.40
FAP-N	7.50	0.23	7.30	7.46	0.1	11.4	6.7	2.2	−10.3	−3.52
FAP-O	7.50	0.23	5.90	6.78	0.1	12.6	7.4	2.5	−10.2	−6.62
FAP-P	7.50	0.23	4.97	6.26	0.1	15.5	9.1	3.1	−10.2	−9.91
CFA-3A*	0.77	0.21	2.98	4.40	<0.002	782	433	173	−9.90	−19.0
CFA-3B*	0.87	0.21	5.02	7.09	<0.002	35.8	20.1	7.8	−11.3	−7.27
CFA-9A*	0.31	0.26	3.03	4.33	<0.002	674	360	162	−9.87	−45.6
CFA-9B*	0.45	0.28	3.00	4.40	<0.002	735	390	181	−9.97	−35.1
CFA-9C*	0.45	0.26	4.80	6.33	<0.002	29.1	16	7.1	−11.4	−39.1
CFA-9D*	0.45	0.26	3.56	5.10	<0.002	167	89.7	39.3	−10.7	−22.9
CFA-10A*	0.51	0.21	3.02	4.50	<0.002	732	376	181	−9.89	−33.1
CFA-10B*	0.99	0.21	5.02	6.77	<0.002	26.9	13.5	6.9	−11.6	−33.3
CFA-1A*	0.30	0.29	3.01	4.85	<0.002	795	385	210	−9.59	−35.4

* Performed in fluidized bed reactor.

a function of pH (Table 3). The dissolution rate of FAP as a function of pH appears to have two distinct slopes with the change in slope occurring at $5 < pH < 6$ (Fig. 6). Log mineral dissolution rates that demonstrate a linear dependence on pH can be described using the log of the equation (Blum and Lasaga, 1988):

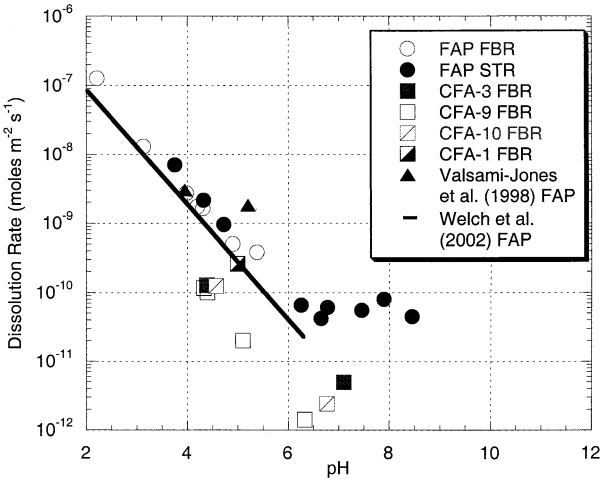

Fig. 6. Experimental apatite dissolution rates as a function of pH and composition.

$$R = k\{H^+\}^n, \quad (7)$$

where

R = dissolution rate (moles m^{-2} s^{-1})
k = rate constant (moles m^{-2} s^{-1})
H^+ = hydrogen ion activity
n = reaction order.

Using this equation from $2 < pH < 5.5$, the calculated rate constant k is 5.75×10^{-6} mol m^{-2} s^{-1} and n is −0.81 with $r^2 = 0.98$. Using Eqn. 7 from $6.0 < pH < 8.5$, the calculated rate constant k is 6.53×10^{-11} mol m^{-2} s^{-1} and n is −0.01 with $r^2 = 0.004$. Thus, the data suggest a strong dissolution rate dependence on pH for FAP from $2 < pH < 5.5$ after which the dissolution rate is essentially invariant from $6.0 < pH < 8.5$. Although there are fewer data points for CFA, the trend of all compositions between $4 < pH < 7$ fit with a linear regression yielding a rate constant $k = 6.91 \times 10^{-8}$ mol m^{-2} s^{-1} and $n = -0.67$ with $r^2 = 0.79$. The variation in the dissolution rate as a function of pH of the four CFA compositions is likely related to compositional differences (e.g., the amount of CO_3 substitution) between the CFA compositions used in this study. However it should be noted that ΔG_R (see below section 3.4 Degree of Undersaturation) can have an influence on the dissolution rate of apatite at a given pH. This must also be taken into account when comparing rates at different pHs between

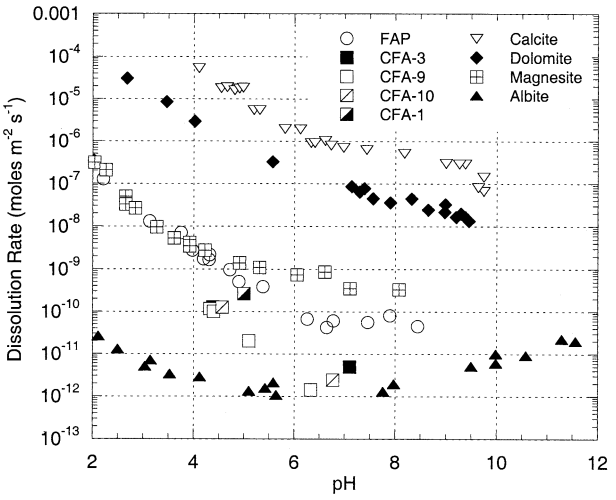

Fig. 7. Mineral dissolution rates as a function of pH [The FAP and CFA rates are from this study. The calcite, dolomite and magnesite rates are from Chou et al. (1989), and the albite rates from Chou and Wollast (1985)].

FAP and CFA compositions, as in section 3.3 Apatite Composition Comparison.

The dissolution rate behavior of FAP over the acidic pH range (2.0–6.0) is similar to that of certain carbonate phases such as calcite, dolomite, and magnesite (Fig. 7). Both FAP and these carbonate phases demonstrate a log-linear decrease in dissolution rate with an increase in pH up to an inflection point between $5.5 < pH < 6.5$. However, after this inflection point and proceeding to higher pHs, the dissolution rate for FAP is relatively invariant with increasing pH. In comparison, the dissolution rate of carbonates after the inflection point continues to decrease with increasing pH, but not at the same rate as in the acidic pH range.

As mentioned previously, the inflection point for FAP occurs approximately at $pH = 6.0 \pm 0.5$. One possible reason for the change in slope in this near neutral pH region is related to changes in the relative concentrations of hydroxylated mineral surface groups as a function of pH. Wu et al. (1991) demonstrated that $\equiv PO^-$ and $\equiv CaOH_2^+$ are the dominant charged surface complexes for hydroxylated FAP and that their populations are pH dependent. Starting at $pH = 4.5$ and with increasing pH, $\equiv PO^-$ becomes an important charged surface group for FAP. For example comparing experimental results at $pH = 6.0$ and 7.0, 25 and 70%, respectively, of the total phosphate surface complex population (comprised of $\equiv PO^-$ and $\equiv POH$) are $\equiv PO^-$ surface sites. This is a large change in the relative $\equiv PO^-$ percentage of the total phosphate surface complex population over a small pH range, and suggests that the substantial increase in $\equiv PO^-$ population may control the dissolution rate in this pH region. Below $pH = 7.2$, all the calcium surface complex population is $\cdot CaOH_2^+$. Therefore, there are no changes in the relative population of $\cdot CaOH_2^+$ from $6 < pH < 7$, further suggesting that $\equiv PO^-$ controls the rate in this pH region.

Other researchers have been able to correlate dissolution rate with changes in pH. With albite, the slope of the dissolution rate vs. pH curve in both acidic and basic pH ranges was demonstrated to correlate very well with the slope of the surface concentration of H^+ and OH^- vs. pH (Blum and Lasaga, 1988). For both forsterite (Pokrovsky and Schott, 2000) and enstatite (Oelkers and Schott, 2001), the dissolution rate decreases going from acidic to basic pH.

There are few previously published dissolution experiments on apatite compositions similar to those used in this work with which to compare the dissolution rates of this study. Figure 6 shows a comparison of available data (Valsami-Jones et al., 1998; Guidry and Mackenzie, 2000; Welch et al., 2002). Valsami-Jones et al., (1998) investigated with batch reactor experiments synthetic hydroxyapatite and natural fluorapatite dissolution in the presence of aqueous metal cations over a range of pH. In 0.1 mol/L $NaNO_3$ at a $pH = 3.95 \pm 0.15$ and 5.2 ± 0.2, they calculated the dissolution rate of natural fluorapatite to be 3.0×10^{-9} and 1.83×10^{-9} mol m^{-2} s^{-1}, respectively. As can be seen in Figure 6, the Valsami-Jones et al. (1998) rate at $pH = 3.95$ is very similar to the rate of the current study and to that of Welch et al. (2002). However, the Valsami-Jones et al. (1998) rate at $pH = 5.2$, is approximately 5 times faster than the rate found in the current study. This difference in rates at this pH could be due to a number of factors such as the difference in the reactor types used in the two studies, variation in medium ($NaNO_3$ vs. NaCl), experiments being performed at different chemical affinities, and the degree of undersaturation at which the dissolution reaction rates were obtained. Deriving dissolution rates from batch reactors can be problematic because the reactor solution composition varies over the course of the reaction. In addition, for the Valsami-Jones et al. (1998) experiment at $pH = 5.2$, only dissolved Ca was measured (dissolved Ca and PO_4 concentrations were measured for the $pH = 3.95$ experiment), and the dissolution reaction was presumed to be stoichiometric. In the event the reaction was not congruent, then their rate calculated on the basis of Ca concentration is likely to be high. This is due to the elevated initial release of Ca during the early stages of the dissolution reaction because of the exchange of solution H^+ for solid-bound Ca at acidic pH; a phenomenon discussed in the following section on reaction congruency.

Welch et al. (2002) investigated the effects of microorganisms and microbial metabolites on natural FAP dissolution rates over a range of pH using batch reactors. To provide a baseline for their study, Welch et al. (2002) studied the effect of pH on the rate of FAP dissolution from $2 < pH < 7$. The regression fit ($k = 5.7 \times 10^{-6}$ moles m^{-2} s^{-1}, $n = -0.87$, $r^2 = 0.94$) of the Welch et al. (2002) dissolution rate vs. pH data for their inorganic FAP dissolution experiments is plotted in Figure 6. From $2 < pH < 5$, the regression line for the Welch et al. (2002) data set is in good agreement with the overlapping fluidized bed and stirred tank reactor data of this study. From $5 < pH < 6.5$, the Welch et al. (2002) regression line deviates from the data trend of this study, although the considerable scatter in their data over this pH region suggests that the dissolution rate was invariant with change in pH. It is also possible that the scatter was related to artifacts associated with batch reactor experiments. Welch et al. (2002) did not investigate the response of the dissolution rate at $pH > 6.5$, so it was not possible to compare the data from this study from $6.5 < pH < 8.5$ with any previous experimental work on natural FAP dissolution rates.

3.3. Apatite Composition Comparison

Although both FAP and CFA are apatites, they have different thermodynamic and kinetic properties due to the highly substituted nature of CFA, even though FAP can contain impurities as well. CFA can have relatively elevated amounts of CO_3, SO_4, Na, and Mg along with trace amounts of K, Ag, Ba, Sr, Cd, Mn, Zn, Bi, Sc, Y, REEs, U, V, Si, and Br substituted into the mineral lattice (e.g., Glenn et al., 1994). Depositional and postdepositional temperature and solution compositions determine the degree of elemental substitutions in CFA (for an extensive review of CFA geochemistry and formation see Glenn et al., 1994 and Jarvis et al., 1994). These substitutions and their degree give rise to the variation in solubility between FAP and all CFA compositions. Jahnke (1985) studied the solubility differences of laboratory synthesized FAP and CFA with variable degrees of CO_3 substitution. FAP was found to have the lowest solubility (log K ~ -122). CFA with the maximum CO_3 substitution ($\sim$ 6.5 wt. %) was found to have the highest solubility (log K ~ -107.5).

Over the pH range 4–7, FAP dissolves faster than three of the four CFA compositions (Fig. 3), although the effect of ΔG_R on the dissolution rate was not taken into account. In addition to ΔG_R concerns, there are at least two caveats to using these results to conclude that FAP dissolves faster than CFA over this pH range. The first caveat is that the difference in the ionic strength of reacted solution between the FAP and CFA solution experiments should be considered. The FAP dissolution experiments were conducted at I = 0.1, whereas the CFA dissolution experiments were conducted at I $\leq$ 0.002. Increases in solution ionic strength can both decrease (e.g., Stillings and Brantley, 1995) and increase (e.g., Icenhower and Dove, 2000) mineral dissolution rates. Increases in ionic strength can reduce the dissolution rate because of competitive absorption between cations and hydrogen ions at mineral surface exchange sites. Cation ion adsorption inhibits hydrogen ion absorption thus reducing dissolution rates. In H_2O-HCl-NaCl solutions, dissolution rates of feldspar decreased with increasing ionic strength due to sodium ion preferentially binding to surface dissolution sites (e.g., Stillings and Brantley, 1995). Increase in ionic strength can also increase the dissolution rates of a mineral. This results from the effect of ionic strength on solution saturation state. The higher ionic strength solution will tend to cause the degree of undersaturation of the solution relative to the dissolving mineral to increase relative to a lower ionic strength solution due to the formation of ionic complexes. Therefore, the saturation state of the higher ionic strength solution is pushed in the direction of greater undersaturation compared to the lower ionic strength solution, which should lead to faster rates. For example, Icenhower and Dove (2000) demonstrated that amorphous silica dissolution rates at near-neutral pH solutions were enhanced by over an order of magnitude in a solution with I = 0.05 compared to amorphous silica dissolution rates in deionized water where the ionic strength is essentially zero.

The second caveat is that the FAP and CFA grains were treated differently in their preparation. To produce the size fractionated FAP grains (106–212 μm) for the dissolution experiments, it was necessary to hand grind larger FAP pieces into smaller pieces of FAP using an agate mortar and pestle. No grinding was necessary to obtain the CFA 106–212 μm grain size fraction. The grinding of mineral solid by pestle mortar can create excess surface free energy (e.g., ultrafine particles, microfractures, sharp edges, kinks, etc.) and thus additional surfaces sites where dissolution could take place (e.g., Holdren and Berner, 1979; Petrovic, 1981). SEM revealed that the sonication treatment of the FAP grains removed any ultrafine particles resulting from grinding. In addition, the grinding process may have introduced additional dislocations, which could have increased the dissolution rate depending on the distance from equilibrium of the reaction (e.g., Lee et al., 1998).

A number of researchers (e.g., Lasaga and Blum, 1986; Hochella and Banfield, 1995 and Lee et al., 1998) have suggested that dislocation sites play a relatively more important role in field weathering as opposed to laboratory experimental weathering. One reason for this assertion is that most laboratory dissolution experiments take place at highly undersaturated conditions. Under highly undersaturated conditions, all dissolution surface sites actively participate in the dissolution reaction. As the solution becomes more saturated, only those sites with lower activation energies of dissolution will contribute to the dissolution process as demonstrated by Lee et al., (1998) for alkali feldspars. Given that most of our dissolution rate data were likely collected under relatively far-from-equilibrium conditions, it is probable that any additional surface dissolution sites created by grinding did not significantly influence the dissolution rate.

There is some variability in the CFA dissolution rates at higher pH that may be due to variation in CFA composition (see Table 2). Although perhaps counterintuitive, the more soluble CFA need not dissolve faster than the relatively less soluble FAP at the same pH. For example, although magnesite (log $K_{sp} = -8.20$) and calcite (log $K_{sp} = -8.48$) are both simple carbonates displaying similar solubilities, their dissolution rates can vary by 3–4 orders of magnitude from $4 < pH < 8$ (Chou et al., 1989). The differences in dissolution rates between calcite and magnesite are in part due to the fact that it is difficult to hydrate magnesite and also to dehydrate the Mg^{2+} ion in solution (Chou et al., 1989).

3.4. Degree of Undersaturation

During the past decade, there has been an increasing interest in determining how mineral dissolution rates can vary, sometimes widely, over a broad range of undersaturation conditions (e.g., Nagy et al., 1991; Nagy and Lasaga, 1992; Burch et al., 1993; Cama et al., 1999). The effect of varying the degree of undersaturation on FAP dissolution was investigated at 25°C, pH = 3.0, I = 0.1, and $pCO_2 = 0$ using the stirred tank reactor (Fig. 8). The dissolution rate of FAP varies in a nonlinear fashion with respect to the degree of undersaturation in a similar fashion as albite, gibbsite, labradorite, and smectite (for summary see Lasaga and Luttge, 2001). The dissolution rate of FAP was found to vary by $\sim 5\times$ from $\Delta G_R = -20$ to -30 kcal/mol under the experimental conditions. An understanding of how the degree of undersaturation affects dissolution rates is also important in determining the apparent activation energy, E_a, of dissolution for a mineral. Cama et al., (1999) demonstrated that variation in E_a determinations for kaolinite disso-

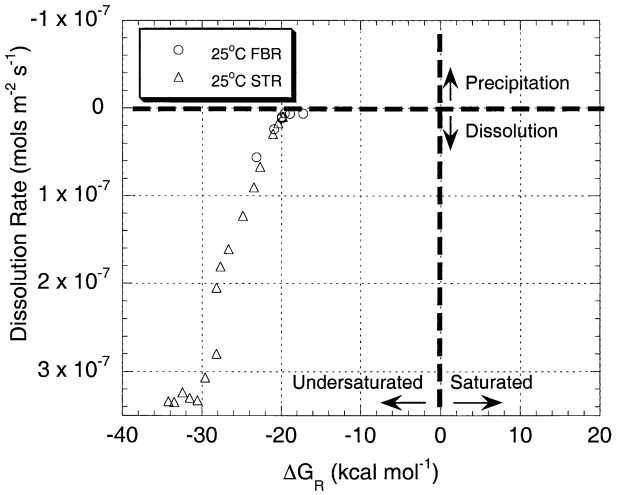

Fig. 8. ΔG_R effects on FAP dissolution rates at pH = 3.0, I = 0.1 and 25°C. Note that the y-axis is compressed close to zero so that the dissolution rate appears to go to zero around $\Delta G_R = -20$ kcal mol^{-1}.

lution is attributable to experimental dissolution rates collected over a wide range of undersaturations, not all of which were obtained in the rate-invariant dissolution plateau region. Although the effect was not investigated in this study, recent work (Pokrovsky and Schott, 1999; 2000; Oelkers, 2001; Oelkers and Schott, 2001) has demonstrated that rates at a given pH for certain minerals are actually dependent upon the aqueous activity of a single species at a given pH rather than the composite activity of solution species (i.e., ΔG_R) at a given pH.

3.5. Apparent Activation Energy of Dissolution

As discussed above, the degree of undersaturation can have an impact on dissolution rates. To determine the E_a of FAP dissolution, experiments over a range of solution conditions undersaturated with respect to FAP at 35 and 55°C were conducted to combine with the 25°C results (Fig. 9a and Table 4). The dissolution plateau rates—i.e., the area of undersaturation far from equilibrium where rates are invariant with increasing undersaturation—for 25, 35, and 55°C experiments were then used to compute the E_a of dissolution. It was important to ensure that the 35 and 55°C rates were in the dissolution plateau area due to the complicating fact that FAP exhibits retrograde or reverse solubility, which results in the solubility decreasing with increasing temperature. For minerals with retrograde solubility, the accompanying reduction in the solubility of the mineral counteracts the increased dissolution rate due to increased temperature. It is interesting to note that at all three temperatures (25, 35, and 55°C), the dissolution plateau occurs in the same ΔG_R region ($\Delta G_R < -30$ kcal mol^{-1}). The E_a calculated from these experiments is 8.3 ± 0.2 kcal mol-1 (Fig. 9b). This E_a for apatite is similar to that measured for calcite from 5 to 50°C (8.4 kcal mol^{-1}; Sjöberg, 1976) and is greater than activation energies of diffusion controlled reactions ($E_a <$ 5 kcal mol^{-1}; Lasaga, 1998), suggesting a surface controlled reaction for apatite dissolution.

If properly conducted, kinetic experimental studies of min-

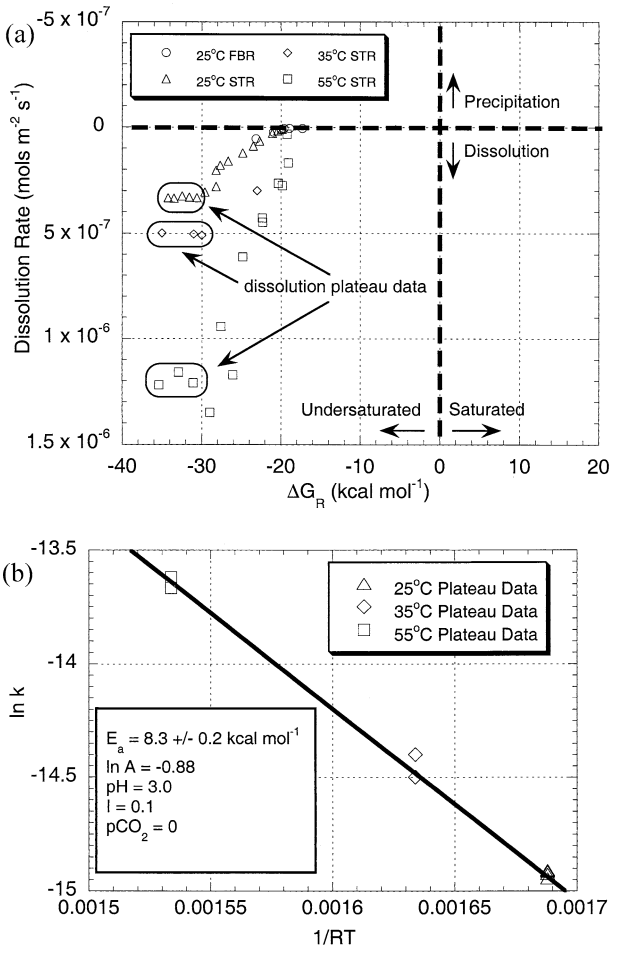

Fig. 9. A. ΔG_R effects on FAP dissolution rates at pH = 3.0, I = 0.1, at 25, 35 and 55°C. Note that the y-axis is compressed close to zero so that the dissolution rate appears to go to zero around $\Delta G_R = -20$ kcal mol^{-1}. Figure 9B. Apparent activation energy of FAP dissolution determined from dissolution plateau rates at 25, 35, and 55°C in Figure 9A.

erals can yield information about fundamental mineral properties. The information can then be used to assist in modeling processes associated with the mineral. Van Cappellen and Berner (1991) experimentally studied the crystal growth rate of FAP under simple seawater conditions. They used the experimental results to predict the size that an apatite particle would grow to as it was buried in marine sediment. Arvidson and Mackenzie (1999) used their experimental results of the effect of temperature and solution composition on dolomite precipitation rates to model how variation in seawater composition and temperature influenced the abundance of dolomite in the sedimentary rock record. In the next section, the experimental results of pH and temperature effects on FAP dissolution rates are used to investigate how the long-term P flux from apatite weathering may have changed with variation in average global temperature and rock surface area over the Phanerozoic. The temporal variation in long-term P flux is related to the timing of late Proterozoic and Phanerozoic phosphorite and evolutionary events.

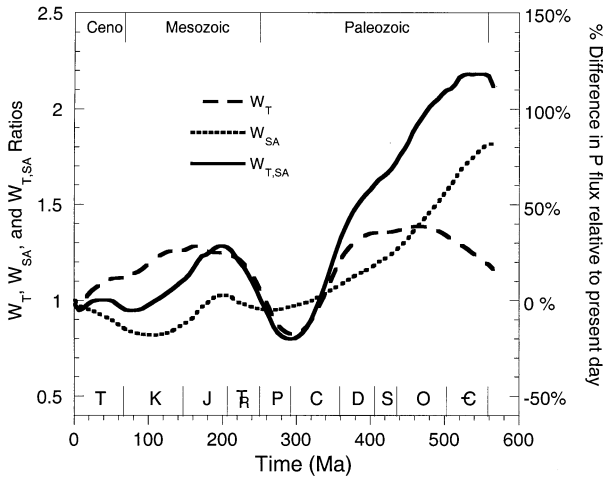

Fig. 10. Sensitivity of the phosphorus flux from inorganic apatite weathering to Phanerozoic variation in average global temperature and igneous rock surface area. W_T is the effect of variation in temperature alone using the experimentally determined apparent activation energy of dissolution (8.3 kcal mol^{-1}), W_{SA} is the effect of variation in surface area alone, and $W_{T,\ SA}$ is the combined effect of variation in both temperature and surface area on the phosphorus weathering flux. Note that there are no provisions for organic effects on apatite dissolution in the apatite weathering model formulation. Original model formulation is in Guidry and Mackenzie (2000).

3.6. Application of Experimental Results: Long-term P Flux from Apatite Weathering

The chemical weathering of continental material, containing apatite as the primary P phase, controls the long-term availability of phosphorus (e.g., Garrels and Mackenzie, 1971; Garrels et al., 1975; Holland, 1984; Delaney, 1998; Guidry et al., 2000). Phosphorus availability is thought to control long-term marine net ecosystem production (e.g., Tyrrell, 1999). Therefore, the rate of weathering and subsequent release of P from apatite plays an important role in regulating long-term marine net ecosystem production. Chemical weathering rates are a function of many variables (e.g., temperature, pH, and organic acid concentrations—see Lasaga et al., 1994 for review), which is why mineral dissolution experiments are useful because they can quantify and separate out the effects of these sometimes interrelated variables.

Guidry and Mackenzie (2000) modeled how variation in temperature and rock surface area at a fixed pH may have influenced the long-term weathering of apatite over the Phanerozoic (see Guidry and Mackenzie, 2000 for details of model formulation). This apatite weathering model has been rerun here incorporating the experimentally determined activation energy value of FAP dissolution from this study (Fig. 10). The objective of these model runs was not to compute actual P fluxes over time, but rather to investigate the sensitivity of the P weathering flux to changes in temperature and surface area individually and then to both temperature and surface area combined relative to the present-day flux. The combined effects of Phanerozoic variation in average global temperature (using E_a = 8.3 kcal mol^{-1}) and igneous rock surface area, $W_{T,SA}$, relative to present day were determined by the following ratio:

$$W_{T,\,SA} = \frac{p(t)T_v,\ SA_v}{p(t)T_c,\ SA_c}, \tag{8}$$

where

$p(t)_{Tv}$,SA_v = the P flux from apatite weathering with average global temperature and igneous rock surface area varying over the Phanerozoic.

$p(t)_{Tc}$,SA_c = the P flux from apatite weathering at fixed present-day temperature, 15°C, and fixed present-day igneous rock surface area.

In addition, for reference to our earlier work (Guidry and Mackenzie, 2000), we have also plotted (Fig. 10) the values of W_{SA} and W_T. W_{SA}—the effect of Phanerozoic variation in apatite surface area normalized to present-day apatite surface area on the phosphorus flux from apatite weathering—is the same as Guidry and Mackenzie (2000) because the surface area formulation was not changed. The updated W_T calculation—the effect of Phanerozoic variation in average global temperature normalized to present-day average global temperature on the phosphorus flux from apatite weathering—using the experimentally determined E_a (8.3 kcal mol^{-1}) falls within the W_T sensitivity analyses using E_a = 5, 10, and 15 kcal mol^{-1} of Guidry and Mackenzie (2000).

The $W_{T,SA}$ calculation results exhibit three general features. The first feature is that from the early Cambrian to the mid-Carboniferous, the P flux from apatite weathering was elevated relative to the present-day flux. In the early Cambrian, the P weathering flux reached its maximum value of 120% or 2.2 times greater than that of the present-day flux. The elevated P flux over this interval is due to both elevated average global temperature and surface area relative to present-day average global temperature and surface area. An interesting application of this model result, especially the highly elevated early Cambrian P flux, is with regard to the Snowball Earth Hypothesis (Hoffman et al., 1998). The most striking climatic aspect of this hypothesis is the oscillation between long-term (millions of years) global glaciation followed by a catastrophic switch (over a period of hundreds to thousands of years) to global greenhouse conditions. These extreme global glaciations and rapid switching to global greenhouse conditions occurred before the rapid diversification of multicellular life from 525 to 575 million years ago termed the Cambrian explosion. The long periods of isolation and extreme environments on a Snowball Earth may have spurred on genetic change and could help account for this evolutionary burst.

Supplementing this climatic evolutionary pressure that perhaps stimulated the Cambrian explosion is a concomitant sustained elevated P weathering flux during the early Phanerozoic, as calculated using the apatite-weathering model. The near equatorial configuration of the continents, which places much of the continental weathering surface in the warm low latitudes, and the elevated average global temperatures of the early Paleozoic would have resulted in an elevated P weathering flux from apatite dissolution. Given the lack of rooted plants and associated physical and chemical facilitation of rock and mineral dissolution by biota at this time, the surface area available for weathering and the average global temperature probably were more important during this interval of time than during the post-Devonian in controlling apatite weathering rates.

There is other support from the geologic record of the apatite weathering model results suggesting elevated P riverine fluxes during the early Paleozoic. First, there is fossil evidence for elevated P availability given the abundance and diversity of phosphatic-shelled species at the Precambrian-Cambrian boundary and during the early Cambrian (e.g., Brasier, 1992). P as a controlling nutrient is important for organic production and so proliferation and survival of these phosphatic-shelled organisms along with other metazoans suggests that the P weathering flux to the oceans in the early Cambrian was elevated. Second, there are extensive phosphatic sediment deposits, phosphorites, during the Precambrian-Cambrian interval (e.g., Cook and McElhinny, 1979). Shields et al. (2000) argue that many of these Precambrian-Cambrian phosphorite deposits were accompanied by increased global weathering rates and thus P input to the ocean, although other paleoceanographic factors such as ocean ventilation rates and degree of anoxia (e.g., Colman, 1994; Colman and Holland, 1994; Van Cappellen and Ingall, 1994) may have been important in controlling marine P concentrations. Derry et al., (1992) demonstrated that the global positive $\delta^{13}C_{carbonate}$ event from 590 to 550 Ma was accompanied by elevated $^{87}Sr/^{86}Sr$ values. This suggests that elevated continental weathering, e.g., apatite weathering, resulted in increased terrestrial nutrient input, e.g., P, which subsequently resulted in elevated organic carbon production and burial causing the positive $\delta^{13}C_{carbonate}$ event.

The second feature of the model results is from the mid-Carboniferous through the Permian (Fig. 10). During this interval, there was a reduction in the P weathering flux, up to 20% at the Permo-Carboniferous boundary, relative to present day due to a pronounced reduction in average global temperature compared to the rest of the Phanerozoic. At the Permo-Carboniferous boundary, the Geocarb II model of Berner (1994) computes the average global temperature to be approximately 8 to 9°C. This interval of the Phanerozoic may have experienced the lowest P flux owing to global temperature and surface area effects on apatite weathering even though one of the largest Phanerozoic phosphorite deposits—i.e., the Permian Phosphoria Formation—formed during this time. While previously mentioned factors such as ocean ventilation and anoxia may have been important in the deposition of large scale phosphorite formations such as the Phosphoria Formation (e.g., Glenn et al., 1994), it is likely that the rise and spread of rooted vascular plants during the Devonian may have also played a role.

While this model serves to illustrate the effect of temperature and surface area on the weathering flux of P, it does so in an inorganic world—i.e., one for which there are no influences such as plants, bacteria, and organic acids on weathering and dissolution. The rise and spread of rooted vascular plants during the Devonian are likely to have accelerated the weathering of rocks and associated minerals (e.g., Lovelock and Whitfield, 1982; Algeo et al., 1995; Berner, 1997). In addition, organic acids resulting from decaying plant detrital matter, exudates of plant roots and rootlets, and bacterially mediated mineral dissolution can accelerate rock and mineral dissolution rates (e.g., White and Brantley, 1995). These model results need to be examined with these caveats in mind, especially for the post-Devonian where rooted vascular land plants and organic acids produced by them likely enhanced apatite weathering rates and the resulting P flux from land to ocean. If the Permian Phosphoria formation was a result, at least in part, of a long-term sustained elevated P flux from apatite weathering, it was likely that enhanced weathering due to the rise of rooted vascular land plants offset the low global average temperature effects on apatite weathering.

The final feature of the model results is that other than the local P flux peak at the Jurassic-Triassic boundary, the P flux from apatite weathering owing to Mesozoic-Cenozoic variation in average global temperature and surface area is similar to the present-day flux. From the present day until the mid-Cretaceous, the reduced surface area available for weathering counteracts the elevated temperatures enhancing the dissolution rate. From the mid-Cretaceous to the Jurassic-Triassic boundary, the elevated temperatures coupled with an increase in surface area resulted in a P weathering flux that was 30% greater than the present-day flux.

4. CONCLUSIONS

FAP and CFA dissolution was incongruent in the early stages, but tended toward congruency as the dissolution reaction proceeded to steady state. The initial incongruency was likely a result of the exchange of solution H^+ ion for mineral bound Ca. This exchange reaction has also been observed for silicate minerals such as albite. The initial incongruency results in elevated solution Ca:P and Ca:F ratios compared to mineral stoichiometry and increased solution pH in the early regime of the dissolution reaction. The dissolution rates of FAP and CFA are highly dependent on pH, and FAP releases components faster than CFA at a given pH even though it has a lower solubility. The FAP and CFA dissolution rates fall between those of the more reactive carbonates –calcite and dolomite— and the less reactive silicates—e.g., albite. The apparent activation energy of dissolution for FAP coupled with the early incongruent dissolution reaction suggests that FAP and CFA dissolution is a surface controlled process. The degree of undersaturation has a considerable effect on the dissolution rate of FAP. Given the retrograde solubility characteristic of apatite, the degree of undersaturation must be taken into account when determining the E_a of FAP dissolution.

An apatite weathering model using the experimental results of this study was employed to investigate the effects of Phanerozoic variation in average global temperature and apatite surface area on the P flux from apatite weathering. The model results demonstrate that Phanerozoic variation in both temperature and surface area likely had significant effects on the P flux from apatite weathering. The elevated surface area and temperatures during the early Phanerozoic led to relatively elevated P weathering fluxes. Early Phanerozoic elevated P weathering fluxes may have assisted in the rapid diversification of multicellular organisms—i.e., the Cambrian explosion—and large-scale phosphorite deposition during this interval of time.

Acknowledgments—This work was supported by the donors of The Petroleum Research Fund administered by the American Chemical Society, by a grant-in-aid of research from Sigma Xi, the scientific research society, and by a research grant from the Geological Society of America. We thank Steve Smith, Jane Tribble, and Craig Glenn for their input and review of the initial manuscript. The paper benefited greatly from the editorial review and handling by Eric Oelkers and the

Table 4. Degree of undersaturation experiments at pH = 3.0, I = 0.1, and 25, 35, and 55°C. 106–212 μm FAP was used for all experiments. Input pH measured at 25°C for all experiments. Output pH for all experiments measured at 25°C and then extrapolated to elevated temperature using EQ3 if the dissolution reaction was at 35 or 55°C. Experiments using the STR are italicized.

Exp.	Solid (g)	Input rate (g min^{-1})	pH		Temp. (°C)	Steady State Ca, P, and F (μmol kg-sln^{-1})			Log Rate (mol m^{-2} s^{-1})	ΔG_R (kcal mol^{-1})
			Input	Ouput		Ca	P	F		
M	1.0	0.38	2.80	3.05	25	234	142	46.5	−7.93	−19.9
P	1.0	0.91	2.87	3.04	25	195	117	38.3	−7.61	−20.9
Q	1.0	3.12	2.95	3.03	25	134	80.1	25.9	−7.25	−23.1
T	1.0	0.18	2.72	2.95	25	253	148	50.8	−8.19	−19.6
S2	0.50	0.12	2.75	2.95	25	311	187	61.5	−7.99	−19.8
T2	0.50	0.23	2.78	2.96	25	290	166	56.2	−7.76	−20.4
U2	0.50	0.43	2.85	2.95	25	246	148	48.6	−7.53	−21.1
V2	0.50	1.33	2.89	2.95	25	181	109	35.7	−7.17	−22.7
W2	0.50	2.11	2.91	3.01	25	151	94.1	29.3	−7.04	−23.5
X2	0.50	3.73	2.90	3.02	25	119	74.2	24.3	−6.91	−24.8
Y2	0.50	6.72	2.91	2.99	25	85.9	49.7	16.8	−6.79	−26.6
Z2	0.50	9.33	2.95	2.99	25	68.4	41.3	13.2	−6.74	−27.6
A3	0.50	11.8	2.95	2.98	25	62.8	37.7	12.7	−6.69	−28.2
D3	0.10	3.20	2.89	3.01	25	55.4	32.8	11.3	−6.55	−28.2
E3	0.10	4.55	2.89	2.99	25	46.9	28.1	9.1	−6.51	−29.6
F3	0.10	6.00	2.93	2.98	25	41.6	24.1	8.1	−6.48	−30.6
G3	0.10	7.25	2.94	2.99	25	32.1	19.3	6.2	−6.48	−31.5
H3	0.10	8.27	2.95	3.00	25	28	16.6	5.5	−6.49	−32.5
I3	0.10	10.5	2.95	2.98	25	22.7	13.8	4.5	−6.48	−33.5
J3	0.10	12.0	2.94	2.97	25	19.6	11.8	3.7	−6.48	−34.2
H4	0.05	7.52	2.96	3.05	35	24.8	14.8	4.9	−6.30	−31.0
I4	0.05	9.30	2.98	3.02	35	23.1	13.8	3.4	−6.30	−35.0
J4	0.05	10.0	3.00	3.05	35	20.1	11.6	3.8	−6.29	−30.0
K4	3.00	2.10	2.92	3.04	35	545	315	106	−7.28	−23.0
S3	0.05	3.76	2.98	3.04	55	117	69.3	22.8	−5.93	−26.1
T3	0.05	9.23	2.97	3.02	55	51.1	29.4	10	−5.92	−31.1
U3	0.05	15.1	2.99	3.01	55	31	17.4	5.9	−5.91	−35.4
V3	0.11	14.8	2.95	2.98	55	77	42	15	−5.87	−29.0
W3	0.11	8.33	2.95	3.02	55	88	53	17.6	−6.02	−27.6
X3	0.11	3.43	2.93	2.97	55	141	84	27.4	−6.21	−24.8
Y3	0.11	2.10	2.93	3.01	55	192	114	37.4	−6.37	−22.3
Z3	0.50	7.55	2.81	3.01	55	215	128	41.8	−6.35	−22.3
A4	0.50	3.20	2.80	3.00	55	299	183	59.6	−6.58	−20.3
B4	0.50	1.64	2.76	2.92	55	372	219	74	−6.77	−19.0
C4	1.0	6.10	2.80	2.99	55	333	195	66.2	−6.56	−19.8
D4	1.0	0.66	2.76	2.97	55	360	216	71.1	−7.49	−19.2
F4	0.05	11.7	2.91	2.95	55	36.7	22.1	6.9	−5.94	−32.9

efforts of three anonymous reviewers. School of Ocean and Earth Science and Technology (SOEST) Contribution 6139.

Associate editor: E. Oelkers

REFERENCES

Algeo T. J., Berner R. A., Maynard J. B., and Scheckler S. E. (1995) Late Devonian oceanic anoxic events and biotic crises: "Rooted"in the evolution of vascular land plants? *GSA Today* **5**, 45–66.

Arvidson R. S. (1998) The kinetics of dolomite precipitation with application to changes in seawater saturation state over the past 100 Ma. Ph. D. thesis, University of Hawaii at Manoa.

Arvidson R. S. and Mackenzie F. T. (1999) The dolomite problem: control of precipitation kinetics by temperature and saturation state. *Am. J. Sci.* **299**, 257–288.

Berner R. A. (1994) Geocarb II: a revised model of atmospheric CO_2 over Phanerozoic time. *Am. J. Sci.* **294**, 1–56.

Berner R. A. (1997) The rise of plants and their effect on weathering and atmospheric CO_2. *Science* **276**, 544–546.

Blum A. E. and Lasaga A. C. (1988) Role of surface speciation in the low temperature dissolution of minerals. *Nature* **331**, 431–433.

Brasier M. D. (1992) Nutrient-enriched waters and the early skeletal fossil record. *J. Geol. Soc. London* **149**, 621–629.

Budz J. A. and Nancollas G. H. (1988) The mechanism of dissolution of hydroxyapatite and carbonated apatite in acidic solutions. *J. Cryst. Growth.* **91**, 490–496.

Burch T. E., Nagy K. L., and Lasaga A. C. (1993) Free energy dependence of albite dissolution kinetics at 80°C and pH 8.8. *Chem. Geol.* **105**, 137–162.

Cama J., Ayora C., and Lasaga A. C. (1999) The deviation-from-equilibrium effect on dissolution rate and on apparent variations in activation energy. *Geochim. Cosmochim. Acta* **63**, 2481–2486.

Chin K. O. A. and Nancollas G. H. (1991) Dissolution of Fluorapatite. A constant-composition kinetics study. *Langmuir* **7**, 2175–2179.

Chin K. O. A., Johnsson M., Bergey E. J., Levine M. J., and Nancollas G. H. (1993) A constant composition kinetics study of the influence of salivary cystatins, statherin, amylase and human serum albumin on hydroxyapatite dissolution. *Coll. Surf. A: Physicochem. Eng. Asp.* **78**, 229–234.

Christoffersen M. R., Dohrup J., and Christoffersen J. (1998) Kinetics of growth and dissolution of calcium hydroxyapatite in suspensions with variable calcium to phosphate ratio. *J. Cryst. Growth.* **186**, 283–290.

Chou L. (1985) Study of the kinetics and mechanisms of dissolution of albite at room temperature and pressure. Ph. D. thesis, Northwestern Univ.

Chou L. and Wollast R. (1984) Study of the weathering of albite at room temperature and pressure with a fluidized bed reactor. *Geochim. Cosmochim. Acta* **48**, 2205–2217.

Chou L. and Wollast R. (1985) Steady-state kinetics and dissolution mechanism of albite. *Am. J. Sci.* **285**, 963–993.

Chou L., Garrels R. M., and Wollast R. (1989) Comparative study of the kinetics and mechanisms of dissolution of carbonate minerals. *Chem. Geol.* **78**, 269–282.

Colman A. S. (1994) Benthic phosphorus regeneration: The global diffusive flux of phosphorus from marine sediments into the oceans and the control of atmospheric oxygen levels throughout the Phanerozoic. Unpublished Senior thesis, Harvard Univ.

Colman A. S. and Holland H. D. (1994) The global diffusive flux of phosphorus from marine sediments into the oceans (abs). *Eos.* **75**, 96.

Compton J., Mallinson D., Glenn C., Filippelli G., Follmi K., Shields G. and Zanin Y. (2000) Variations in the global phosphorus cycle. In *Marine Authigenesis: From global to microbial: SEPM (Society for Sedimentary Geology) Special Publication 66* (eds. C.R. Glenn. L. Prévôt-Lucas, and J. Lucas). pp. 21–33.

Cook P. J. and McElhinney M. W. (1979) A reevaluation of the spatial and temporal deposition of sedimentary deposits in the light of plate tectonics. *Econ. Geol.* **74**, 315–330.

Delaney M. L. (1998) Phosphorus accumulation in marine sediments and the oceanic phosphorus cycle. *Glb. Biogeochem. Cycles* **12**, 563–572.

Derry L. A., Kaufman A. J., and Jacobsen S. B. (1992) Sedimentary cycling and environmental change in the Late Proterozoic: Evidence from stable and radiogenic isotopes. *Geochim. Cosmochim. Acta* **56**, 1317–1329.

Dorozhkin S. V. (1997) Surface Reactions of Apatite Dissolution. *J. Coll. Inter. Sci.* **191**, 489–497.

Froelich P. N., Bender M. L., Luedtke N. A., Heath G. R., and DeVries T. (1982) The marine phosphorus cycle. *Am. J. Sci.* **282**, 474–511.

Froelich P. N., Kim K. H., Jahnke R., Burnett W. C., Soutar A., and Deakin M. (1983) Pore water fluoride in Peru continental margin sediments: Uptake from seawater. *Geochim. Cosmochim. Acta* **47**, 1605–1612.

Garrels R. M. and Mackenzie F. T. (1971) Evolution of sedimentary rocks. W.W. Norton, New York.

Garrels R. M., Mackenzie F. T., and Hunt C. (1975) Chemical cycles and the global environment: Assessing human influence. William Kaufman Inc., Los Altos.

Glenn C. R., Föllmi K. B., Riggs S. R., Baturin G. N., Grimm K. A., Trappe J., Abed A. M., Galli-Olivier C., Garrison R. E., Ilyin A. V., Jehl C., Rohrlich V., Sadaqah R. M. Y., Schidlowski M., Sheldon R. E., and Seigmund H. (1994) Phosphorus and phosphorites: Sedimentology and environments of formation. *Eclogae geologicae Helvetiae.* **87**, 747–788.

Guidry M. W. and Mackenzie F. T. (2000) Apatite weathering and the Phanerozoic phosphorus cycle. *Geology* **28**, 631–634.

Guidry M. W., Mackenzie F. T. and Arvidson R. S. (2000) Role of tectonics in phosphorus distribution and cycling. In *Marine Authigenesis: From global to microbial: SEPM (Society for Sedimentary Geology) Special Publication 66*(eds. C.R. Glenn. L. Prévôt-Lucas, and J. Lucas). pp. 35–51.

Gulbrandsen R. A. (1970) Relation of carbon dioxide content of apatite of the Phosphoria Formation to regional facies. *USGS Prof. Paper* **700-B,** p. 9–13.

Hochella M. F. Jr. and Banfield J. F. (1995)Chemical weathering of silicates in nature: A microscopic perspective with theoretical considerations. In *Chemical Weathering Rates of Silicate Minerals* (ed. A.F. White and S.L. Brantley) *Am. Min. Soc. Rev. Mineral.* 31, 353–406.

Hoffman P. F., Kaufman A. J., Halverson G. P., and Schrag D. P. (1998) A Neoproterozoic snowball Earth. *Science* **281**, 1342–1346.

Holdren G. J. and Berner R. A. (1979) Mechanism of feldspar weathering. I. Experimental studies. *Geochim. Cosmochim Acta* **43**, 1161–1171.

Holland H. D. (1984) The chemical evolution of the atmosphere and oceans. Princeton University Press, Princeton.

Icenhower J. P. and Dove P. M. (2000) The dissolution kinetics of amorphous silica into sodium chloride solutions: Effects of temperature and ionic strength. *Geochim. Cosmochim. Acta* **64**, 4193–4203.

Jahnke R. A. (1981) Current phosphorite formation and the solubility of synthetic carbonate fluorapatite. Ph. D. thesis, University of Washington.

Jahnke R. A. (1985) The synthesis and solubility of carbonate fluorapatite. *Am. J. Sci.* **284**, 58–78.

Jarvis I., Burnett W. C., Nathan Y., Almbaydin F. S. M., Attia A. K. M., Castro L. N., Flicoteaux R., Ezzeldim Hilmy M., Husain V., Qutawnah A. A., Serjani A., and Zanin Y. N. (1994) Phosphorite geochemistry: State-of-the-art and environmental concerns. *Eclogae geologicae Helvetiae.* **87**, 643–700.

Koroleff F. (1983) Chap. 9. Determination of phosphorus. In *Methods of Seawater Analysis* 2nd edition (eds. K. Grasshoff, M. Ehrhardt, and K. Kremling), pp. 125–139. Verlag Chemie, Weinheim. .

Lane M. III and Mackenzie F. T. (1990) Mechanisms and rates of natural carbonate fluorapatite dissolution. *Geological Society of American Abstracts with Programs* **21,** *6*, A208.

Lane M. III and Mackenzie F. T. (1991) Kinetics of carbonate fluorapatite dissolution: Application to natural systems. *Geological Society of American Abstracts with Programs* **22**(7), A151.

Lasaga A. C. and Blum A. E. (1986) Surface chemistry, etch pits and mineral-water reactions. *Geochim. Cosmochim. Acta* **50**, 2363–2379.

Lasaga A. C., Soler J. M., Ganor J., Burch T. E., and Nagy K. L. (1994) Chemical weathering rate laws and global geochemical cycles. *Geochim. Cosmochim. Acta* **58**, 2361–2386.

Lasaga A. C. (1998) Kinetic theory in the Earth Sciences. Princeton University Press, Princeton.

Lasaga A. and Luttge A. (2001) Variation of crystal dissolution rate based on a dissolution stepwave model. *Science* **291**, 2400–2404.

Lee M. R., Hodson M. E., and Parsons I. (1998) The role of intragranular microtextures and microstructures in chemical and mechanical weathering: Direct comparisons of experimentally and naturally weathered alkali feldspars. *Geochim. Cosmochim. Acta* **62**, 2771–2788.

Lovelock J. E. and Whitfield M. (1982) Life span of the biosphere. *Nature* **296**, 561–563.

McClellan G. H. and Lehr J. R. (1969) Crystal chemical investigation of natural apatites. *Am. Mineral.* **54**, 1374–1391.

McClellan G. H. (1980) Mineralogy of carbonate fluorapatites. *J. Geol. Soc. London* **137**, 675–681.

Nagy K. L., Blum A. E., and Lasaga A. C. (1991) Dissolution and precipitation kinetics of kaolinite at 80°C and pH 3: The dependence on solution saturation state. *Am. J. Sci.* **291**, 649–686.

Nagy K. L. and Lasaga A. C. (1992) Dissolution and precipitation kinetics of gibbsite at 80°C and pH 3: The dependence on solution saturation state. *Geochim. Cosmochim. Acta* **56**, 3093–3111.

Oelkers E. H. (2001) General kinetic description of multioxide silicate mineral and glass dissolution. *Geochim. Cosmochim. Acta* **65**, 3703–3719.

Oelkers E. H. and Schott J. (2001) An experimental study of enstatite dissolution rates as a function pH, temperature, and aqueous Mg and Si concentration, and the mechanism of pyroxene/pyroxenoid dissolution. *Geochim. Cosmochim. Acta* **65**, 1219–1231.

Petrovic R. (1981) Kinetics of dissolution of mechanically comminuted rock forming oxides and silicates: I. Deformation and dissolution of quartz under laboratory conditions. *Geochim. Cosmochim. Acta* **45**, 1665–1674.

Pokrovsky O. S. and Schott J. (2001) Kinetics and mechanism of dolomite dissolution in neutral to alkaline solutions revisited. *Am. J. Sci.* **301**, 597–626.

Pokrovsky O. S. and Schott J. (2000) Kinetics and mechanisms of forsterite dissolution at 25°C and pH from 1 to 12. *Geochim. Cosmochim. Acta* **64**, 3313–3325.

Robie R. A., Hemingway B. S., and Fisher J. R. (1979) Thermodynamic properties of minerals and related substances at 298.15K and 1 bar (10^5 Pascals) pressure and at higher temperatures: U.S.G.S. Bull. 1452 (with corrections). **1452,** 1456p.

Ruttenberg K. C. (1993) Reassessment of the oceanic residence time of phosphorus. *Chem. Geol.* **107**, 405–409.

Schaad Ph., Poumier F., Voegel J. C., and Gramain Ph. (1997) Analysis of calcium hydroxyapatite dissolution in non-stoichiometric solutions. *Coll. Surf. A: Physicochem. Eng. Asp.* **121**, 217–228.

Schuffert J. D., Kastner M., Emanuele G., and Jahnke R. A. (1990) Carbonate-ion substitution in francolite: A new equation. *Geochim. Cosmochim. Acta* **54**, 2323–2328.

Shields G., Stille P. and Brasier M. D. (2000) Isotopic records across two phosphorite giant episodes compared: The Precambrian-Cambrian and the late Cretaceous-recent. In *Marine Authigenesis: From global to microbial: SEPM (Society for Sedimentary Geology) Special Publication 66* (eds. C.R. Glenn. L. Prévôt-Lucas, and J. Lucas). pp. 103–115.

Sjöberg E. L. (1976) A fundamental equation for calcite dissolution kinetics. *Geochim. Cosmochim. Acta* **40**, 441–447.

Smith S. V. (1984) Phosphorus versus nitrogen limitation in the marine environment. *Limnol. Oceanogr.* **29**, 1149–1160.

Stilling L. L. and Brantley S. L. (1995) Feldspar dissolution at 25°C and pH 3: Reaction stoichiometry and the effect of cations. *Geochim. Cosmochim. Acta* **59**, 1483–1496.

Tribble J. S., Lane M. J., Arvidson R. S., and Mackenzie F. T. (1995) Crystal chemistry, and thermodynamic and kinetic properties of calcite, dolomite, apatite, and biogenic silica: applications to petrologic problems. *Sediment. Geol.* **95**, 11–37.

Tyrrell T. (1999) The relative influences of nitrogen and phosphorus on oceanic primary production. *Nature* **400**, 525–531.

Valsami-Jones E., Ragnarsdottir K. V., Putnis A., Bosbach B., Kemp A. J., and Cressey G. (1998) The dissolution of apatite in the presence of aqueous metal cations at pH 2–7. *Chem. Geol.* **151**, 215–233.

Van Cappellen P. and Berner R. A. (1991) Fluorapatite crystal growth from modified seawater solutions. *Geochim. Cosmochim. Acta* **55**, 1219–1234.

Van Cappellen P. and Ingall E. D. (1994) Benthic phosphorus regeneration, net primary production, and ocean anoxia: A model of the coupled marine biogeochemical cycles of carbon and phosphorus. *Paleoceanog.* **9**, 677–692.

Warner T. B. (1969) Fluoride in seawater: measurement with lanthanum fluoride electrode. *Science* **165**, 178–180.

Warner T. B. (1973) Fluoride analysis in seawater and in other complex natural waters using an ion- selective electrode- techniques, potentialities, limitations. In Chemical Analysis of the Environment (eds. S. Ahuja, E.M. Cohen, T.H. Kneip, J.L. Lambert, and G. Zweig) p. 229–240. Plenum Press, New York.

Welch S. A., Taunton A. E., and Banfield J. F. (2002) Effect of microorganisms and microbial metabolites on apatite dissolution. *Geomicrobiol. J.* **19**, 343–367.

White A. F. and Brantley S. L. eds. (1995) Chemical weathering rates of silicate minerals: Mineralogical Society of America Reviews in Mineralogy. **Vol. 31,** 583.pp.

Wolery T. J. (1992) EQ3NR. A computer program for geochemical aqueous speciation-solubility calculations: Theoretical manual, user's guide, and related documentation (version 7.0). Lawrence Livermore National Laboratory. UCRL-MA-110662 PT III.

Wu L., Willis F., and Schindler P. W. (1991) Surface complexation of calcium minerals in aqueous solution. *J. Coll. Inter. Sci.* **147**, 178–185.